RESEARCH ARTICLE

Bimetallic Cu/Ru/Os Complexes: Observation of Conformational Differences Between the Solution Phase and Solid State by Atomic Pair Distribution Function Analysis

Zhu-Lin Xie,[a] Xiaolin Liu,[b] Andrew J. S. Valentine,[b] Vincent M. Lynch,[c] David M. Tiede,[a] Xiaosong Li,*[b] Karen L. Mulfort*[a]

[a] Dr. Z.-L. Xie, Dr. D. M. Tiede, Dr. K. L. Mulfort
Division of Chemical Sciences and Engineering, Argonne National Laboratory.
9700 S Cass Ave, Lemont, IL 60439, United States
E-mail: mulfort@anl.gov
[b] Mr. X. Liu, Dr. A. J. S. Valentine, Prof. Dr. X. Li
Department of Chemistry, University of Washington.
109 Bagley Hall, Seattle, WA 98195-1700, United States
E-mail: xsli@uw.edu
[c] Dr. V. M. Lynch
Department of Chemistry, University of Texas at Austin.
105 E 24TH ST., Austin, TX 78712-1224, United States

Supporting information for this article is given via a link at the end of the document

Abstract: High-energy X-ray scattering and pair distribution function analysis (HEXS/PDF) is a powerful method to reveal the structure of materials lacking long-range order, but is underutilized for molecular complexes in solution. Here we demonstrate the application of HEXS/PDF with 0.26 Å resolution to uncover the solution structure of five bimetallic Os(II)/Ru(II)/Cu(I) complexes. HEXS/PDF of each complex in acetonitrile solution confirms the pairwise distances in the local coordination sphere of each metal center as well as the metal···metal distances separated by over 12 Å. The metal···metal distance detected in solution is compared with that from the crystal structure and molecular models to confirm that distortions to the metal bridging ligand are unique to the solid state. This work presents the first example of observing sub-Å conformational differences by direct comparison of solution phase and solid-state structures and shows the potential for HEXS/PDF in the determination of solution structure of single molecules.

Introduction

Transition metal complexes (TMCs) have a rich diversity in structure arising from the versatility of coordination with ligands and donors from across the periodic table which enables their application in a broad range of areas such as catalysis, light harvesting, magnetism, chemical absorption and separations.[1–5] As such, a key goal of research involving TMCs is to reveal the correlations that dictate how function follows molecular form. However, a complicating factor to accurately mapping activity in response to structure is that TMCs are typically used in a solution phase or complex environment that inhibit identification of molecular structure because of the lack of proper tools to directly probe the structure and particularly how it may change in a dynamic environment.

X-ray scattering characterization can fill in the gaps encountered with traditional methods of molecular structure confirmation (e.g. NMR, mass spectrometry, single-crystal X-ray diffraction). As a global, all-atom characterization technique, X-ray scattering can be used for pair distribution function (PDF) analysis, a Fourier transform of the oscillations observed in reciprocal space to yield pairwise atomic distances in real space.[6–9] By refining simulated structural models to the experimentally measured one-dimensional PDF patterns, one can directly visualize molecular structure. As a result, X-ray scattering has been extensively applied to a wide variety of molecular materials including polymers[10,11], metal oxides[12–18], biomacromolecules[19–22], aggregates of organic compounds[23–25] and supramolecular architectures[26–34].

Advancements at synchrotron X-ray sources have enabled high energy X-ray scattering (HEXS) capabilities, which drastically expands the q range up to ~40 Å^{-1} and yields an achievable spatial resolution of ~0.1 Å.[35] This renders atomic resolution PDF analysis applicable to a wide range of samples[36–39] and has revealed detailed structure information comparable to solid state X-ray diffraction. Petkov et al.[40] have demonstrated that HEXS/PDF can effectively uncover phase identity, relative abundance, and atomic structure from weakly scattering, low-Z disordered materials. Tiede et al. have used HEXS/PDF to determine the atomic-level structure and domain size of thin films of an amorphous cobalt-based water oxidation catalyst material and link domain size with choice of anion.[12,18] HEXS/PDF has also been applied to probe structure in more technically demanding solution environments. For example, the speciation of lanthanide/actinide ions in water has been revealed by HEXS/PDF and has provided insights into the mechanisms of metal ion precipitation from solution phase.[41–44] In battery materials, using HEXS/PDF complexation of metal ions with solvent molecules or counterions have been discovered to be responsible for the special electrochemical stability and ion-

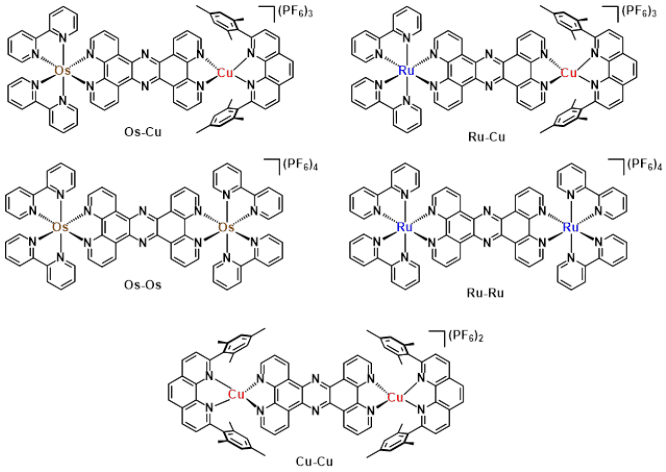

Scheme 1. Chemical structures of the hetero- and homobimetallic complexes studied in this work. All five complexes are bridged by the conjugated tetrapyrido[3,2-*a*:2',3'-*c*:3'',2''-*h*:2''',3'''-*j*]phenazine (tpphz) ligand. Photoactive Cu, Ru or Os metal centers are installed on both sides of tpphz ligand.

conduction mechanism of electrolytes.[45,46] HEXS/PDF analysis has also uncovered solvent restructuring at the surface of nanoparticles which has important implications for materials function and has expanded the tunable parameter space for optimizing activity.[47,48] As these examples show, HEXS/PDF is an effective method for the structural determination of discrete molecules and clusters in the solid and solution state. However, HEXS/PDF analysis is yet not routinely applied to monitor structure of solution phase (supra)molecular complexes with a well-defined ligand motif. Most investigations in TMCs still heavily rely on low-temperature single crystal X-ray diffraction as a proxy for solution structure when rationalizing properties.

In this work, we have used HEXS/PDF with 0.26 Å spatial resolution to investigate the solution phase structure of five bimetallic complexes (**Scheme 1**) consisting of Cu(I)/Ru(II)/Os(II) metal centers connected by the conjugated tetrapyrido[3,2-*a*:2',3'-*c*:3'',2''-*h*:2''',3'''-*j*]phenazine (tpphz) in acetonitrile. The solution phase PDFs for these five complexes confirm the local coordination environment of each metal center, distances in the second coordination sphere, and the long-range metal···metal distances across tpphz. Computational modelling has helped rationalize discrepancies in long-range distances between the solution and solid state by differences in the conformation of tpphz. This work provides a roadmap for how HEXS/PDF and computational analysis can be used to uncover solution structures of (supra)molecular complexes.

Results and Discussion

Synthesis and characterization in solution state. Previously described bimetallic complexes were prepared according to literature procedures with any modifications described in the Supporting Information (**Scheme S1**, **S2**). The synthesis of the new heterobimetallic complex **Os-Cu** was accomplished following a similar approach to that for **Ru-Cu** with modifications to the published procedure[49,50]. Briefly, the synthesis of **Os-Cu** proceeded using the established heteroleptic phenanthroline (HETPHEN) approach demonstrated to yield analytically pure heteroleptic Cu(I)diimine complexes.[51–53] In non-coordinating dichloromethane, equal equivalents of $[Os(bpy)_2(tpphz)]^{2+}$ and $[Cu(mesPhen)(CH_3CN)_2](PF_6)$ (mesPhen = 2,9-dimesityl-1,10-phenanthroline) were mixed together and metalation proceeds rapidly with high yield. Small impurities in $[Os(bpy)_2(tpphz)]^{2+}$ necessitated several rounds of recrystallization in a mixture of acetonitrile and diethyl ether to obtain the pure product.

^{1}H NMR spectroscopy confirmed the identity and purity of each complex and was used to comment on changes to metal electronic structure or possible aggregation in the bimetallic complexes (**Figures S9**-**S11**). Interestingly, the newly synthesized **Os-Cu** shows that the local chemical environment of the ground state of the Os(II) center is not impacted by that of Cu(I) center as evidenced by negligible shifts in proton resonances between the monometallic and bimetallic complexes (**Figure S9**). We interpret this observation as electronically decoupled local coordination environments, despite their connection through the π-conjugated tpphz ligand. The monometallic $[Os(bpy)_2(tpphz)](PF_6)_2$ shows a concentration-dependence with some proton signals in ^{1}H NMR[50], but such change in chemical shift was not observed in the NMR of any of the bimetallic complexes (**Figure S11**), indicating that supramolecular aggregates are not present in solutions of these bimetallic complexes.

The UV-Vis absorption spectra of **Os-Cu** was measured in acetonitrile (**Figure S13**) and the relevant data are compared with published data for the other homo- and bimetallic complexes in **Table S1**. **Os-Cu** has two absorption features associated with metal-to-ligand charge transfer (MLCT) at a similar wavelength to that of **Os-Os** (**Figure S13**, **Os-Cu**: 431, 478 nm; **Os-Os**: 432, 475 nm) which are assigned to M(d)→tpphz(π*) or M(d)→bpy(π*) transitions. However, the intensity of the two MLCT bands of **Os-Cu** are 15% lower than those of **Os-Os**, which is expected as Cu(I) phenanthroline complexes generally display lower extinction coefficient than Os(II) bipyridine complexes. Like other Os(II)poly(pyridyl) complexes, the absorbance of the MLCT band of **Os-Cu** and **Os-Os** extends to almost 750 nm, which is related to the reduced energy gap between the ground state and the MLCT excited state and the increased intensity of spin-forbidden MLCT transitions (singlet-triplet).[54,55]

The room temperature emission of ($[Os(bpy)_2(tpphz)](PF_6)_2$, **Os-Os**, and **Os-Cu**) was recorded in acetonitrile to compare with previously published results for **Ru-Ru**, **Ru-Cu**, and **Cu-Cu** (**Table S1**, **Figure S14**). $[Os(bpy)_2(tpphz)](PF_6)_2$ and **Os-Cu** are emissive at room temperature with λ_{em} at 735 and 730 nm, respectively, while **Os-Os** is non-emissive. The non-emissive nature of **Os-Os** has previously been attributed to the low excited state energy with respect to the ground state such that the life time of the MLCT state is too short and the radiationless deactivation is dominated at room temperature.[55] Based on previous studies[49,56–58], Cu(I) complexes with 2,9-H substitution are non-emissive at room temperature and therefore the emission of **Os-Cu** most likely originates from the Os(II) center.

Cyclic voltammetry was performed on the Os(II) complexes in acetonitrile (**Figure S15**) and the metal-centered oxidation potentials are summarized in **Table S1**. The Cu(II/I) redox couple occurs at less oxidizing potentials than those of Ru(III/II) and Os(III/II). The $E(Cu^{2+/1+})$ of **Os-Cu** appears at +0.54 V *vs.* SCE, which is slightly lower than the $E(Cu^{2+/1+})$ of **Ru-Cu** and **Cu-Cu** (+0.55 V and +0.58 V *vs.* SCE, respectively). In addition, all the Cu(II/I) redox processes are quasi-reversible as a result of the

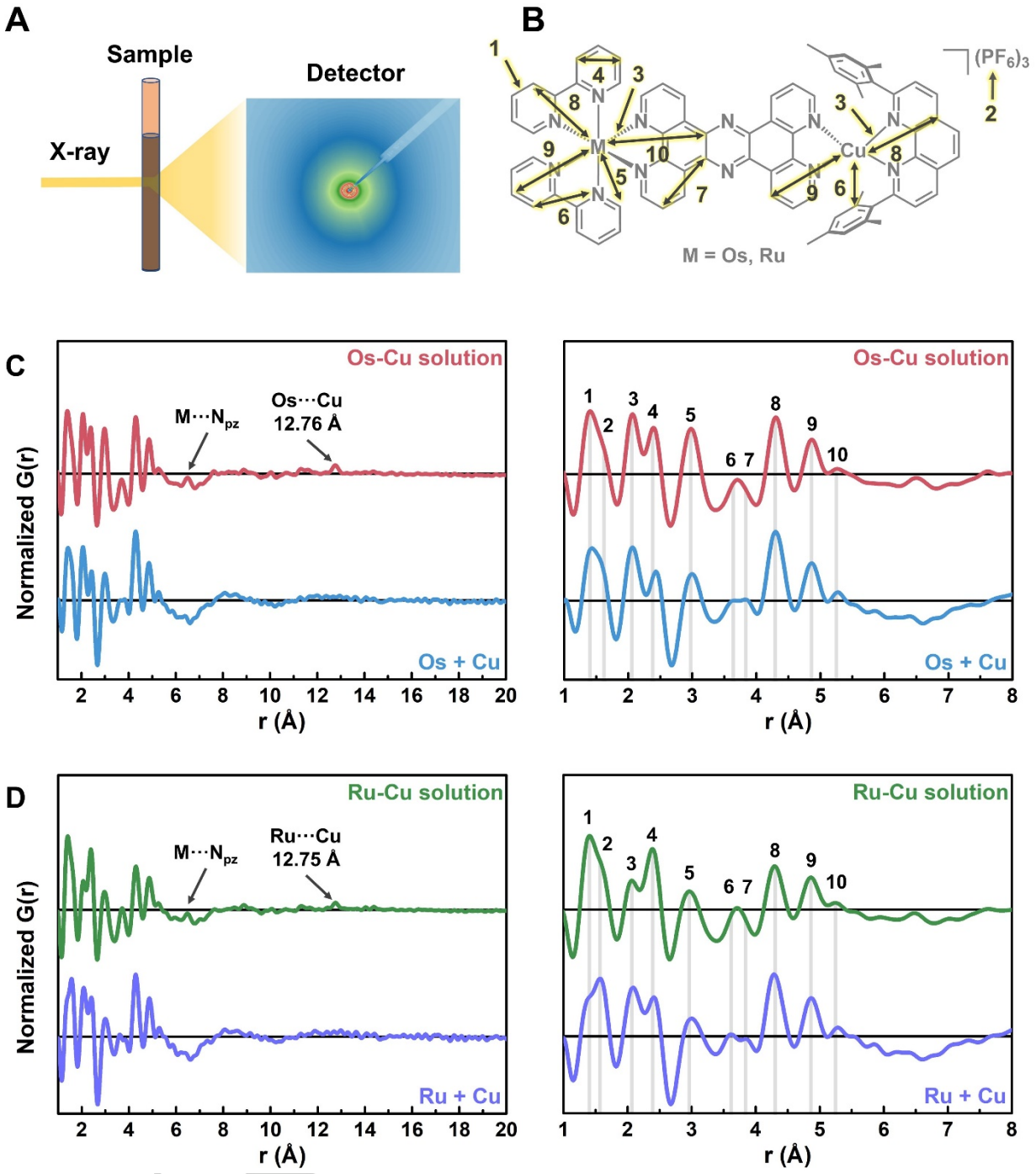

Figure 1. (A) Experimental setup used in solution HEXS/PDF study showing raw detector image acquired at Beamline 11-ID-B of the Advanced Photon Source. (B) Chemical structure of the heterobimetallic complexes in PDF analysis annotated with atomic pairwise distances. (C, D) Comparison of the solution PDF patterns of **Os-Cu** and **Ru-Cu** to sum of relevant monometallic modules. The peaks in the PDFs are assigned to corresponding pairwise distances in the chemical structure. **Os+Cu** stands for the sum of *G*(r) of $[Os(bpy)_2(Phen)](PF_6)_2$ and $[Cu(mesPhen)(Phen)](PF_6)$ and **Ru+Cu** for the sum of *G*(r) of $[Ru(bpy)_2(Phen)](PF_6)_2$ and $[Cu(mesPhen)(Phen)](PF_6)$. All samples were measured at 20 mM concentration in acetonitrile.

flattening distortion of the metal center in Cu(II) state.[59] The Os(III/II) redox potential for **Os-Cu** is +0.90 V *vs.* SCE, comparable to that of **Os-Os** (+0.89 V *vs.* SCE), and 0.43 V more cathodic than the Ru(II/III) couple in Ru(II)tpphz complexes.[49,50]

HEXS/PDF determination of solution structure. The solution phase structure of all five bimetallic complexes and three mononuclear reference complexes was interrogated by HEXS on 20 mM solutions in acetonitrile using 58.6 keV X-rays at Beamline 11-ID-B of the Advanced Photon Source (APS) at Argonne National Laboratory. The sample was charged in Kapton capillary

and the scattering signal was measured in transmission mode as is shown in **Figure 1A**. The high energy X-ray source enabled us to measure the total scattering pattern in reciprocal space, $I(q)$, with a range of 0.5 $Å^{-1} < q < 24 Å^{-1}$. The spatial resolution of the experiment is related to the maximal q value by the equation of $d = 2\pi/q_{max}$, thus this HEXS study achieved spatial resolution of 0.26 Å. PDFgetX2[60] was used to process the raw scattering data and generate the reduced scattering pattern $S(q)$ and the real-space Fourier transform $G(r)$ in real space. Full details for experiment setup and data processing are in the Supporting Information.

The PDF patterns for heterobimetallic **Ru-Cu** and **Os-Cu** are compared with the sum of the $G(r)$ of the relevant mononuclear complexes in **Figure 1B-D**, and the same comparison for the homobimetallic complexes is presented in **Figure S28**. All PDF patterns have several peaks between 1 < r < 6 Å, and we can assign each one to a specific pairwise distance in the first and second coordination shells of the metal centers, as well as the P–F bond from the PF_6^- counterion. The close agreement between $G(r)$ of the mononuclear model complexes and the bimetallic complexes in this region suggests that the tpphz bridging ligand and the distal metal center has little to no impact on local pairwise distances. We can also identify the scattering interaction between each metal center and the central pyrazine N atoms at approximately 6.3 Å. The intensity of each $G(r)$ pattern quickly dampens with increasing r value but for each complex there is a broad featureless hump between 6–10 Å which we assign to the solvation sphere surrounding the molecular complexes. The broadness of this feature suggests that the interactions between each complex and surrounding solvent molecules are fluxional and have little to no short-range order detectable by HEXS/PDF. Notably, in the $G(r)$ of all the bimetallic complexes we observe a peak between 12–13 Å that is completely absent in the mononuclear model complexes. We assign this feature to long-range metal-to-metal distances across the tpphz bridging ligand. Importantly, the order of M···M distance in solution follows with the order of atomic radius of the metal centers, i.e. $d_{Cu\text{-}Cu} < d_{Ru\text{-}Cu} < d_{Os\text{-}Cu} < d_{Ru\text{-}Ru} < d_{Os\text{-}Os}$ (**Table S4**).

The observation and quantification of the M···M distance in solutions of the bimetallic complexes is a convenient handle by which to assess the impact of environmental perturbations on (supra)molecular conformation. The ^{1}H NMR and UV-Vis studies described above indicate that there is no strong *inter*molecular interactions observed with bimetallic complexes in solution phase. Previously, $[Os(bpy)_2(tpphz)]^{2+}$ was reported to show concentration-dependence NMR spectra due to the intermolecular π-π stacking in solution[50,61] but none of the bimetallic complexes exhibit similar effects here (**Figure S11**). We presume that as the steric hindrance on both sides of tpphz increases, the bimetallic complexes cannot approach too closely to adjacent molecules in solution to form strong intermolecular interactions.

Single crystal X-ray diffraction. Since low-temperature single crystal XRD is such a common method of structural characterization and conformation of TMCs, XRD quality single crystals of **Cu-Cu**, **Os-Cu** and **Os-Os** were obtained for the first time, with full details presented in the Supporting Information.[62] These new structures are presented in **Figure 2** and compared with previously described XRD structures of **Ru-Ru**[63] and

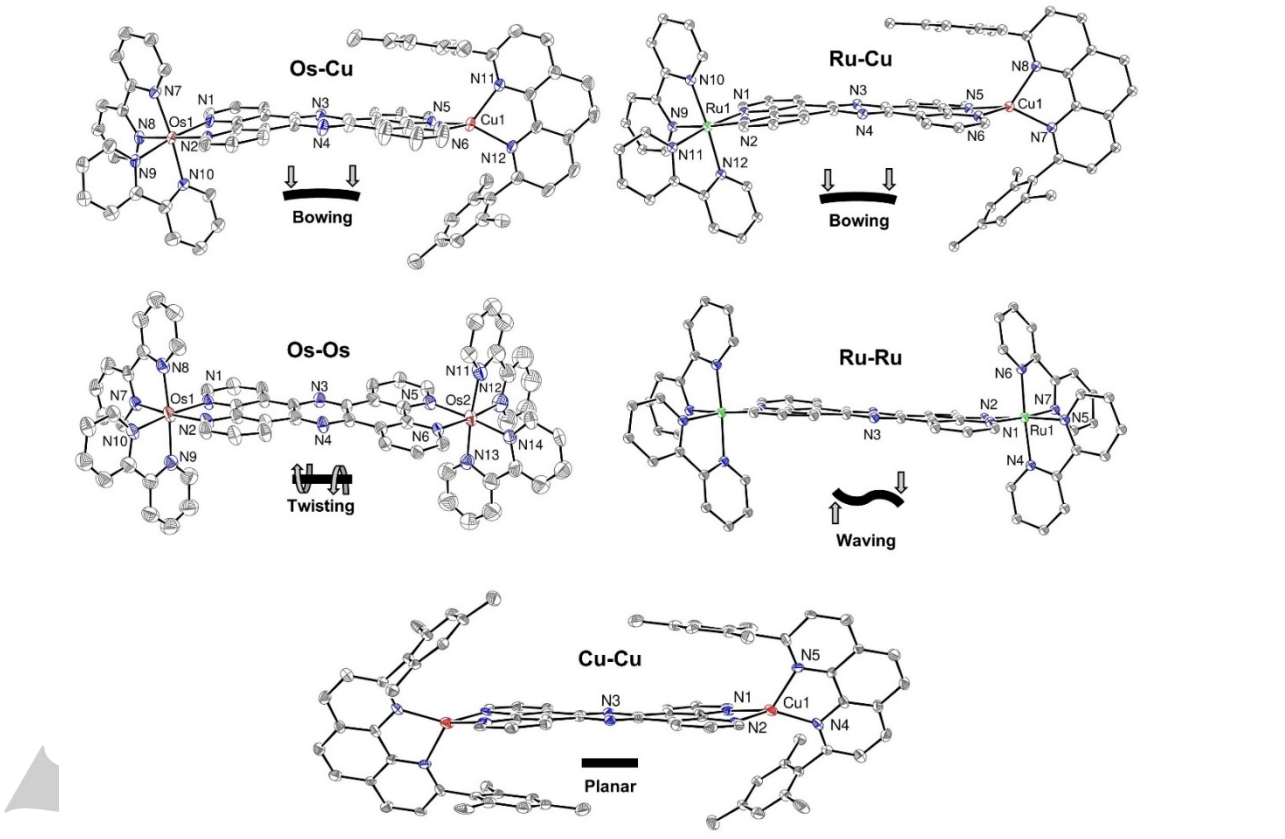

Figure 2. ORTEP diagrams for **Os-Cu**, **Os-Os**, **Ru-Cu**[49], **Ru-Ru**[63] and **Cu-Cu** (30% thermal ellipsoids). H atoms and counterions (Cl^- for **Ru-Ru**, PF_6^- for others) are omitted for clarity.

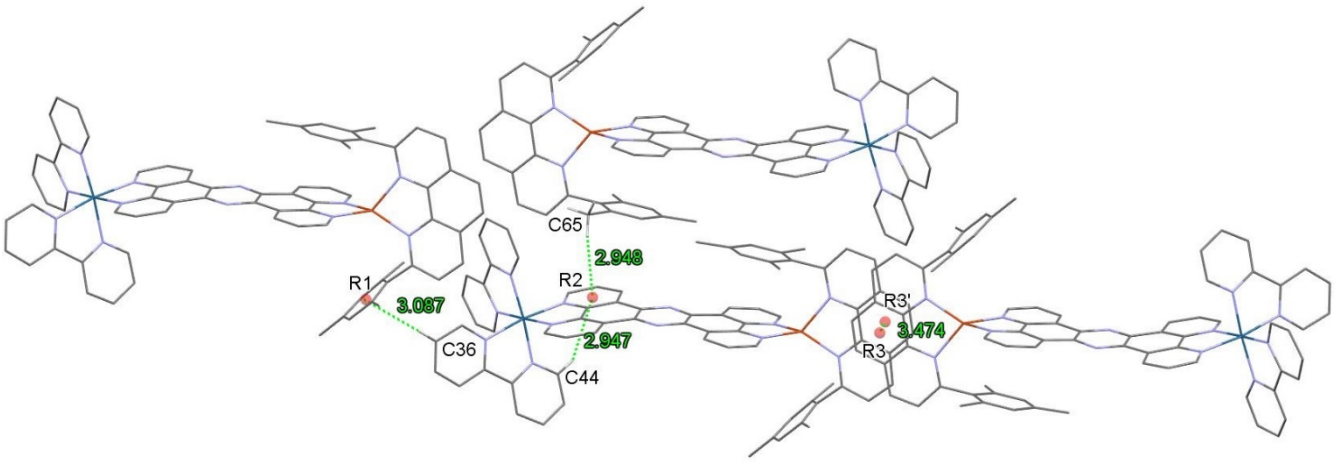

Figure 3. Interactions of **Os-Cu** complexes in crystal lattice that are responsible for the deformation of tpphz. H atoms and counterions (PF_6^-) are omitted for clarity. Numbers in green are distances of specific interactions in Å.

Ru-Cu[49]. As expected, the crystal structures of **Os-Cu** and **Cu-Cu** reveal that the Cu(I) centers are heteroleptically coordinated by mesPhen and tpphz in a pseudotetrahedral geometry, in which the two bidentate ligands are not perpendicular to each other, but slightly flattened. We can quantify the deviation of the geometry from perfect tetrahedral by using the geometry index parameter s_4 which ranges from zero for perfect square planar to one for perfect tetrahedral.[64] The s_4 values for **Os-Cu**, **Ru-Cu** and **Cu-Cu** are 0.715, 0.720 and 0.656 respectively, indicating more deviation from tetrahedral is found in **Cu-Cu** than other two complexes. Like for previous CuHETPHEN crystal structures, intramolecular π-π stacking between one of the mesityl groups of mesPhen with the phenanthroline moiety of tpphz yields the "pac-man" motif at the Cu(I) center.[65,66]. Looking past the local coordination sphere of each metal center, a significant feature of the bridging tpphz ligand is its deviation from planarity in the solid state. We identify three types of deformation of the central ligand: 1) bowing, where the two ends of tpphz bend towards the same direction; 2) twisting, where the two ends of the ligand rotate in opposite directions along the axis containing two metal centers; and 3) waving, where the two ends of the ligand bend towards the opposite direction. The tpphz ligand of **Os-Cu** and **Ru-Cu**[49] both exhibit a bowing deformation (**Figure 2**), with dihedral angle between the two phenanthroline moieties on tpphz (**Figure S17**) calculated as 11.1° and 8.2°, respectively. The complex with a twisting deformation on tpphz is found in **Os-Os**, which gives rise to a dihedral angle of 8.2° between two phenanthroline moieties on tpphz. Despite being a structural congener of **Os-Os**, the central ligand of **Ru-Ru** shows a waving deformation in the crystal structure. Interestingly, in **Cu-Cu**, the tpphz ligand in the crystal structure exhibits only marginal structural variations from planarity.

Analysis of the full XRD structure reveals that various intermolecular forces are responsible for the deformation of tpphz in the bimetallic complexes. For example, in the crystal lattice of **Os-Cu** (**Figure 3**), the mesityl group (ring R1) interacts with the H atom on C36 of another complex, resulting in a C–H···π interaction with a distance of 3.087 Å. Similarly, the R2 ring on tpphz forms C–H···π interactions with C44 and C65 with a distance of 2.947 Å and 2.948 Å, respectively. In addition, π-π interaction of the R3 ring of the mesPhens between adjacent molecules is observed in the crystal lattice. The short distances of these interactions enforce effective repulsions between the two metal centers and induce the bowing conformation of tpphz. The crystal packing patterns of **Ru-Cu** (**Figure S21, S22**) are analogous to those of **Os-Cu**, leading to similar structural distortion in the first coordination shells and the bridging ligand. The single crystal structures of **Ru-Ru** and **Os-Os** also have significant intermolecular interactions which we hypothesize are responsible for the twisting and waving deformations observed in the tpphz ligand of these complexes (**Figure S20**, **S24**). In contrast, there are no intermolecular interactions in the crystal packing of **Cu-Cu** and tpphz in this complex is nearly perfectly planar. From this series of bimetallic complexes we venture that the severe deformations in tpphz are a direct result of *inter*molecular interactions, and in turn substantially impact the *intra*molecular M···M distances observed in the solid state. TheM···M distance of the complexes follows the order of $d_{Os\text{-}Cu} < d_{Ru\text{-}Cu} < d_{Cu\text{-}Cu} < d_{Ru\text{-}Ru} < d_{Os\text{-}Os}$, in contrast with that found from PDF analysis (**Table S3**).

Computational modelling. Energy-minimized DFT models of the bimetallic complexes were generated to help reconcile the differences observed between the M···M distances found from the solution PDF and single crystal XRD structures of the bimetallic complexes, and a comparison of the energy-minimized DFT models with the crystal structures is presented in **Figures 4** and **S45**. DFT calculations were performed using the ωB97X-D functional[67] with the LanL2DZ basis set[68] on transition metals and 6-31G(d) on light atoms. Solvent effects (acetonitrile) were considered using the polarizable continuum model (PCM)[69] to simulate the solvation environment in which the experimental HEXS/PDF study was performed. The hybrid ωB97X-D functional includes Grimme's D2 dispersion correction, which are important for simulation of non-covalent interactions.[67] The most striking difference between the DFT and crystal structures is that all of the optimized, calculated structures of the bimetallic complexes present a flattened tpphz ligand, free of any of the distortions found by single crystal XRD. **Os-Cu** displays the most noticeable difference between the crystal structure and the DFT model: the bend in the tpphz of the crystal

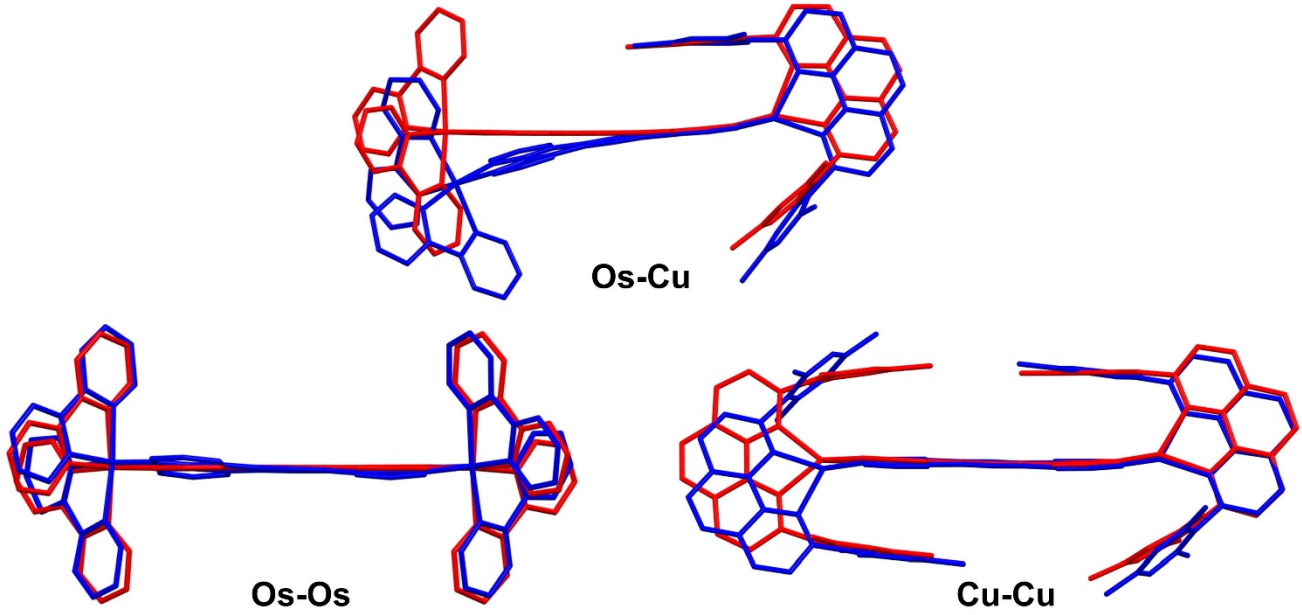

Figure 4. Overlay of the crystal structure (blue) and the DFT optimized structure (red) of **Os-Os**, **Os-Cu** and **Cu-Cu**.

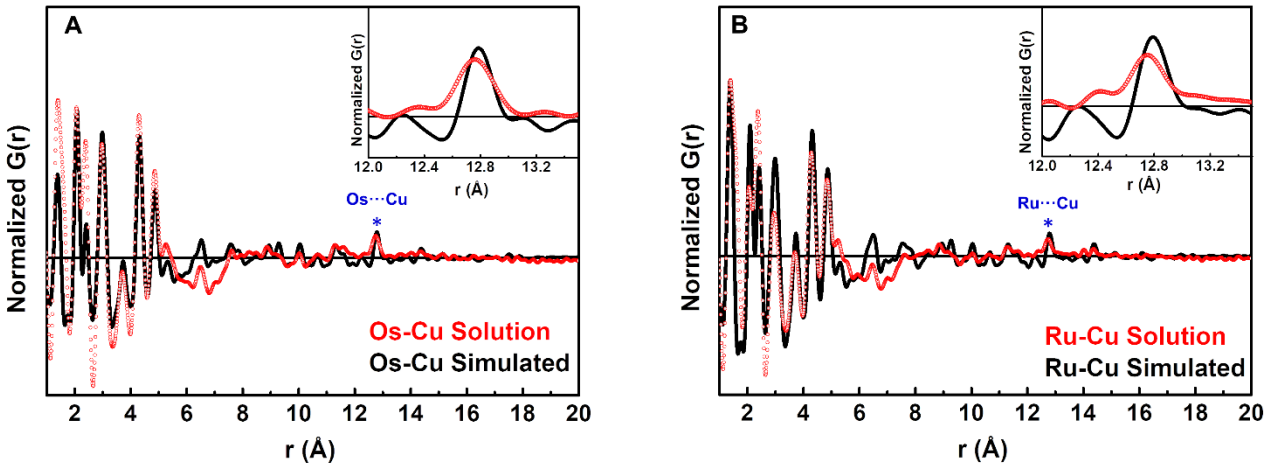

Figure 5. Solution (red dotted line) and calculated (black line) PDF patterns of **Os-Cu** (A) and **Ru-Cu** (B). The inset shows the peak corresponding to the M···M distances.

structure leads to a change of 14.3° in the dihedral angle between the Os(II) module and the Cu(I) module as compared with the DFT model. In the case of the homobimetallic complexes where the tpphz deformations in the solid state are not as severe, the DFT models have a closer resemblance to the solid state but still do not capture the twisting and waving of tpphz found in **Ru-Ru** and **Os-Os**.

To further assess whether the DFT calculations reflect a realistic solution structure, simulated scattering patterns were generated based on the optimized DFT models using SolX[20], and PDF patterns in real space were obtained by Fourier transform of the simulated *I*(q). As compared to the experimentally acquired PDFs (**Figure 5** and **Figure S46**), we note that the simulated and experimental *G*(r) are in excellent agreement in both short and mid-range distances (**Table S5-S9**), with two notable exceptions. First, the solution phase *G*(r) shows a peak at 1.45 Å which we assign to the P–F distance of PF_6^-. The PF_6^- counterions were not included in the DFT simulations since artificially fixing their position with respect to the complexes would lead to meaningless peaks in the simulated PDF. Second, the broad featureless solution sphere interactions seen in the experimental PDFs between 6–10 Å is also absent from the simulated PDF patterns. This is a reasonable discrepancy since the PCM models only reproduce the dielectric response of the solvent and not necessarily semi-ordered solvent surrounding the complexes. Despite these two exceptions, the similarity of the experimental and calculated PDF patterns in the short range (r < 6 Å) indicates that the local coordination spheres of the metal centers in the DFT model structures accurately represent the bonding and molecular geometry in the solution phase.

The M···M distance of the bimetallic complexes is longer in the simulated PDF patterns than those in the solution PDF and

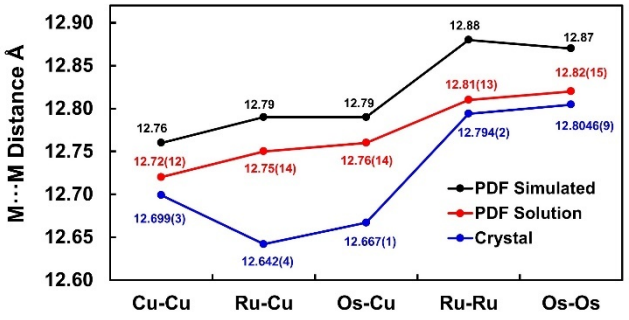

Figure 6. Comparison of the M···M distance of bimetallic complexes in the crystal structure, solution PDF and simulated PDF. The uncertainties of the distances from the solution PDF are shown in parentheses and are estimated by the full-width-at-half-maximum (FWHM) of the peaks corresponding to the M···M distance in *G*(r).

the distance measured in the crystal structure (**Figure 6**). However, the largest difference between the M···M distance observed in the simulated and solution PDFs is only 0.07 Å. This is a remarkably small error considering that the M···M distance covers 10 bonds, translating to a sub-0.01 Å difference per bond as compared to the solution data. The trend in M···M distance found in the DFT models is $d_{Cu\text{-}Cu} << d_{Ru\text{-}Cu} \approx d_{Os\text{-}Cu} << d_{Os\text{-}Os} \approx d_{Ru\text{-}Ru}$, which is the same as the experimental solution PDFs (**Figure 6**). This correlation between the DFT simulations and the solution phase HEXS/PDF measurements strongly suggests that the tpphz ligand of the bimetallic complexes maintains planarity in solution in a sterically relaxed mode.

Interpretation of solution phase PDF by computational models. We can use all of the experimental observations and computational models to describe the solution phase structure and conformation, primarily using the measured and calculated M···M distance as the key metric for comparison. When comparing the M···M distances among the three different structural datasets (solution PDF, solid-state crystal structure, DFT models) we note that the trend in M···M distance of the solution PDF matches that found in the DFT models (**Figure 6**). For the homobimetallic complexes **Cu-Cu**, **Ru-Ru**, and **Os-Os**, the M···M distances observed in the solution PDF agree slightly better with the values from their crystal structures than those of the DFT models (**Figure 6**) (Δ(M···M solution-solid) = 0.02 – 0.03 Å; (Δ(M···M DFT-solution) = 0.04 – 0.07 Å). However, as we can see in **Figure 4** and **Figure S45**, deviations of tpphz from planarity in the solid state of these complexes are quite minimal. From these small and comparable differences between the solid state/solution phase/DFT models it is difficult to distinguish the structure model (solid state or DFT) most closely represents the solution phase structure, since both have a relatively planar tpphz ligand.

For the heterobimetallic complexes **Ru-Cu** and **Os-Cu** which exhibit severe distortions to tpphz in the solid state, we observe a closer agreement between the solution PDF and the DFT models (Δ(M···M solution-solid) = 0.10 – 0.11 Å; (Δ(M···M DFT-solution) = 0.03 – 0.04 Å). This indicates that the extreme bending of tpphz ligand greatly shortens the M···M distance in solid state structure, and the solution state structure should be free from such conformational distortions. Specific considerations for the distortion of tpphz in the solid state structures of **Ru-Cu** and **Os-Cu** is the conformational flexibility of the Cu(I) coordination and the close intermolecular interactions found between the $M(bpy)_2$ modules (where M = Ru(II) or Os(II)), **Figure 3**, **S18**, **S21**, **S22**). It is well documented that Cu(I)bis(phenanthroline) complexes routinely exhibit distortions from perfect tetrahedral geometry, and the severity of which is highly dependent on the 2,9-phenanthroline substitution.[65,66,70] Specifically to **Ru-Cu** and **Os-Cu**, CuHETPHEN model complexes typically favor the "pac-man" orientation in which one mesityl group of mesPhen is stacked with the secondary phenanthroline ligand.[65,66] This has been noted in several crystal structures, but importantly this preferential π-stacking is not observed by other analytical techniques like NMR, and is presumed to be fast on the NMR timescale and therefore a fluxional interaction only resolved in the solid state. Additionally, the relatively small steric bulk of the 2,2'-bpy ligands on Ru(II) and Os(II) allow for close intermolecular π-π interactions in the solid state. We presume that these factors together contribute to the large tpphz distortion in the solid state and therefore the significant difference we observe in the M···M distance measured by measured by solution phase HEXS/PDF.

It is worth noting that this discussion about solution structure is based on models in thermodynamic equilibrium, but we also recognize the kinetic aspect of a molecule in solution and that these TMCs are in a constant state of motion. Indeed, the vibrational modes of the bimetallic complexes corresponding to distortion of tpphz features vibrational frequencies at a magnitude of tens of wavenumber (**Figure S57**). This low value indicates that small perturbations, such as temperature change and solvent interactions, may also induce distortions in tpphz. The solution structure revealed by the HEXS/PDF measurements should be interpreted as an average of the total conformational landscape.

Conclusions

HEXS/PDF analysis was performed on five bimetallic TMCs with photoactive metal centers (Cu(I), Ru(II), and Os(II)) bridged by tpphz to quantitatively determine their solution phase structure and conformation. Spectroscopic analyses demonstrate that the TMCs do not form supramolecular aggregates in solution and that they are free from strong intermolecular interactions. HEXS/PDF analysis of each bimetallic TMC in acetonitrile solution confirmed all of the expected atomic pairwise distances in the first and second coordination shells of each metal center, and we have also observed long-range, over 12 Å, metal···metal distances across the tpphz bridging ligand. The M···M distance from the solution PDF pattern is a convenient experimental observable that we used to compare with solid-state single crystal X-ray structures and DFT models of each bimetallic TMC. The M···M distance found in solution is greater than that found in the solid state, and careful examination of each single crystal structure reveals *inter*molecular interactions between the ancillary ligands of the metal centers which prompts the distortions in tpphz and the observed M···M distance. In a striking contrast to the solid state structures, the DFT models all feature a completely relaxed, planar tpphz ligand. The trend in M···M distance observed in solution by HEXS/PDF follows that found in the DFT models of each isolated bimetallic complex. This correlation, coupled with no spectroscopic evidence for aggregation or intermolecular interactions in solution, lead us to conclude that in solution,

regardless of the metal centers, the bridging tpphz ligand occupies a planar geometry like that found in the DFT models.

To our knowledge, this solution structural study of the bimetallic TMCs is the first report in which HEXS/PDF analysis was used to capture a sub-Å distinction between solution and solid-state structures with resolution comparable to X-ray crystallography. This work demonstrates the unique ability of HEXS/PDF analysis and provides an additional critical tool to describe the structure-function relationship of molecularly-defined materials dissolved in solution. As demonstrated here, low-temperature single crystal XRD fails to accurately depict the solution phase structure of these supramolecular TMCs, which we anticipate will be a general observation as HEXS/PDF is applied more routinely to the interrogation of solution phase molecular structure. This work also sets the foundation for pump-probe studies[71,72] with high resolution in both time and space to visualize the solution structure of molecular samples following perturbation by stimuli such as temperature, applied voltage, and photoexcitation.

Acknowledgements

This work was supported by the Ultrafast X-ray Sciences Initiative in the Solar Photochemistry program of the U.S. Department of Energy, Office of Basic Energy Sciences, Division of Chemical Sciences, Geochemistry, and Biosciences through Contract No. DE-AC02-06CH11357. High-energy X-ray scattering was performed at the Advanced Photon Source, a U.S. Department of Energy (DOE) Office of Science User Facility, operated for the DOE Office of Science by Argonne National Laboratory under Contract No. DE-AC02-06CH11357. The authors thank Dr. Olaf Borkiewicz and Dr. Leighanne Gallington for their expert assistance at Beamline 11-ID-B. This work was facilitated through the use of advanced computational, storage, and networking infrastructure provided by the Hyak supercomputer system and funded by the STF at the University of Washington.

Keywords: X-ray scattering • pair distribution function analysis • X-ray diffraction • structure elucidation • metal-metal interactions

[1] V. W. W. Yam, *Photofunctional Transition Metal Complexes*, Springer Berlin Heidelberg, **2007**.

[2] F. E. Mabbs, D. J. Machin, *Magnetism and Transition Metal Complexes*, Dover Publications, **2008**.

[3] J. R. Gispert, *Coordination Chemistry*, Wiley, **2008**.

[4] D. M. Roundhill, *Photochemistry and Photophysics of Metal Complexes*, Springer US, **2013**.

[5] K. K. W. Lo, *Inorganic and Organometallic Transition Metal Complexes with Biological Molecules and Living Cells*, Elsevier Science, **2016**.

[6] V. Petkov, in *Charact. Mater.*, John Wiley & Sons, Inc., Hoboken, NJ, USA, **2012**, pp. 1–14.

[7] D. M. Tiede, K. L. Mardis, X. Zuo, *Photosynth. Res.* **2009**, *102*, 267–279.

[8] A. Guinier, *X-Ray Diffraction in Crystals, Imperfect Crystals, and Amorphous Bodies*, Dover Publications, **1994**.

[9] L. A. Feigin, D. I. Svergun, L. A. Feigin, D. I. Svergun, G. W. Taylor, in *Struct. Anal. by Small-Angle X-Ray Neutron Scatt.*, Springer US, **1987**, pp. 3–24.

[10] B. Chu, B. S. Hsiao, *Chem. Rev.* **2001**, *101*, 1727–1762.

[11] M. D. Foster, *Crit. Rev. Anal. Chem.* **1993**, *24*, 179–241.

[12] P. Du, O. Kokhan, K. W. Chapman, P. J. Chupas, D. M. Tiede, *J. Am. Chem. Soc.* **2012**, *134*, 11096–11099.

[13] J. Huang, J. D. Blakemore, D. Fazi, O. Kokhan, N. D. Schley, R. H. Crabtree, G. W. Brudvig, D. M. Tiede, *Phys. Chem. Chem. Phys.* **2014**, *16*, 1814–1819.

[14] A. S. Batchellor, G. Kwon, F. A. L. Laskowski, D. M. Tiede, S. W. Boettcher, *J. Phys. Chem. C* **2017**, *121*, 25421–25429.

[15] G. Kwon, H. Jang, J. S. Lee, A. Mane, D. J. Mandia, S. R. Soltau, L. M. Utschig, A. B. F. Martinson, D. M. Tiede, H. Kim, J. Kim, *J. Am. Chem. Soc.* **2018**, *140*, 10710–10720.

[16] X. He, R. Z. Waldman, D. J. Mandia, N. Jeon, N. J. Zaluzec, O. J. Borkiewicz, U. Ruett, S. B. Darling, A. B. F. Martinson, D. M. Tiede, *ACS Nano* **2020**, *14*, 14846–14860.

[17] D. M. Tiede, G. Kwon, X. He, K. L. Mulfort, A. B. F. Martinson, *Nanoscale* **2020**, *12*, 13276–13296.

[18] G. Kwon, O. Kokhan, A. Han, K. W. Chapman, P. J. Chupas, P. Du, D. M. Tiede, *Acta Crystallogr. Sect. B* **2015**, *71*, 713–721.

[19] X. Zuo, D. M. Tiede, *J. Am. Chem. Soc.* **2005**, *127*, 16–17.

[20] X. Zuo, G. Cui, K. M. Merz, L. Zhang, F. D. Lewis, D. M. Tiede, *Proc. Natl. Acad. Sci. U. S. A.* **2006**, *103*, 3534–3539.

[21] R. P. Rambo, J. A. Tainer, *Curr. Opin. Struct. Biol.* **2010**, *20*, 128–137.

[22] J. Lipfert, S. Doniach, *Annu. Rev. Biophys. Biomol. Struct.* **2007**, *36*, 307–327.

[23] B. Rybtchinski, L. E. Sinks, M. R. Wasielewski, *J. Am. Chem. Soc.* **2004**, *126*, 12268–12269.

[24] R. F. Kelley, B. Rybtchinski, M. T. Stone, J. S. Moore, M. R. Wasielewski, *J. Am. Chem. Soc.* **2007**, *129*, 4114–4115.

[25] J. E. Bullock, R. Carmieli, S. M. Mickley, J. Vura-Weis, M. R. Wasielewski, *J. Am. Chem. Soc.* **2009**, *131*, 11919–11929.

[26] D. M. Tiede, R. Zhang, L. X. Chen, L. Yu, J. S. Lindsey, *J. Am. Chem. Soc.* **2004**, *126*, 14054–14062.

[27] T. Megyes, H. Jude, T. Grósz, I. Bakó, T. Radnai, G. Tárkányi, G. Pálinkás, P. J. Stang, *J. Am. Chem. Soc.* **2005**, *127*, 10731–10738.

[28] A. Deák, T. Megyes, G. Tárkányi, P. Király, L. Biczók, G. Pálinkás, P. J. Stang, *J. Am. Chem. Soc.* **2006**, *128*, 12668–12670.

[29] S. J. Lee, K. L. Mulfort, J. L. O'Donnell, X. Zuo, A. J. Goshe, P. J. Wesson, S. T. Nguyen, J. T. Hupp, D. M. Tiede, *Chem. Commun.* **2006**, 4581.

[30] J. L. O'Donnell, X. Zuo, A. J. Goshe, L. Sarkisov, R. Q. Snurr, J. T. Hupp, D. M. Tiede, *J. Am. Chem. Soc.* **2007**, *129*, 1578–1585.

[31] T. Megyes, S. Bálint, I. Bakó, T. Grósz, G. Pálinkás, *J. Am. Chem. Soc.* **2008**, *130*, 9206–9207.

[32] S. J. Lee, K. L. Mulfort, X. Zuo, A. J. Goshe, P. J. Wesson, S. T. Nguyen, J. T. Hupp, D. M. Tiede, *J. Am. Chem. Soc.* **2008**, *130*, 836–838.

[33] E. Holló-Sitkei, G. Tárkányi, L. Párkányi, T. Megyes, G. Besenyei, *Eur. J. Inorg. Chem.* **2008**, *2008*, 1573–1583.
[34] K. L. Mulfort, D. M. Tiede, *J. Phys. Chem. B* **2010**, *114*, 14572–14581.
[35] K. L. Mulfort, A. Mukherjee, O. Kokhan, P. Du, D. M. Tiede, *Chem. Soc. Rev.* **2013**, *42*, 2215–2227.
[36] I. S. Kim, J. Borycz, A. E. Platero-Prats, S. Tussupbayev, T. C. Wang, O. K. Farha, J. T. Hupp, L. Gagliardi, K. W. Chapman, C. J. Cramer, A. B. F. Martinson, *Chem. Mater.* **2015**, *27*, 4772–4778.
[37] A. E. Platero-Prats, Z. Li, L. C. Gallington, A. W. Peters, J. T. Hupp, O. K. Farha, K. W. Chapman, *Faraday Discuss.* **2017**, *201*, 337–350.
[38] J. D. Howe, C. R. Morelock, Y. Jiao, K. W. Chapman, K. S. Walton, D. S. Sholl, *J. Phys. Chem. C* **2017**, *121*, 627–635.
[39] D. Jung, L. M. A. Saleh, Z. J. Berkson, M. F. El-Kady, J. Y. Hwang, N. Mohamed, A. I. Wixtrom, E. Titarenko, Y. Shao, K. McCarthy, J. Guo, I. B. Martini, S. Kraemer, E. C. Wegener, P. Saint-Cricq, B. Ruehle, R. R. Langeslay, M. Delferro, J. L. Brosmer, C. H. Hendon, M. Gallagher-Jones, J. Rodriguez, K. W. Chapman, J. T. Miller, X. Duan, R. B. Kaner, J. I. Zink, B. F. Chmelka, A. M. Spokoyny, *Nat. Mater.* **2018**, *17*, 341–348.
[40] V. Petkov, Y. Ren, S. Kabekkodu, D. Murphy, *Phys. Chem. Chem. Phys.* **2013**, *15*, 8544–8554.
[41] L. Soderholm, S. Skanthakumar, J. Neuefeind, *Anal. Bioanal. Chem.* **2005**, *383*, 48–55.
[42] B. Qiao, S. Skanthakumar, L. Soderholm, *J. Chem. Theory Comput.* **2018**, *14*, 1781–1790.
[43] S. Skanthakumar, G. B. Jin, J. Lin, V. Vallet, L. Soderholm, *J. Phys. Chem. B* **2017**, *121*, 8577–8584.
[44] K. E. Knope, S. Skanthakumar, L. Soderholm, *Inorg. Chem.* **2015**, *54*, 10192–10196.
[45] K. Fujii, M. Matsugami, K. Ueno, K. Ohara, M. Sogawa, T. Utsunomiya, M. Morita, *J. Phys. Chem. C* **2017**, *121*, 22720–22726.
[46] J. Zheng, G. Tan, P. Shan, T. Liu, J. Hu, Y. Feng, L. Yang, M. Zhang, Z. Chen, Y. Lin, J. Lu, J. C. Neuefeind, Y. Ren, K. Amine, L. W. Wang, K. Xu, F. Pan, *Chem* **2018**, *4*, 2872–2882.
[47] M. Zobel, R. B. Neder, S. A. J. Kimber, *Science* **2015**, *347*, 292–294.
[48] M. Zobel, *Acta Crystallogr. Sect. A* **2016**, *72*, 621–631.
[49] D. Hayes, L. Kohler, R. G. Hadt, X. Zhang, C. Liu, K. L. Mulfort, L. X. Chen, *Chem. Sci.* **2018**, *9*, 860–875.
[50] J. Bolger, A. Gourdon, E. Ishow, J.-P. Launay, *Inorg. Chem.* **1996**, *35*, 2937–2944.
[51] M. Schmittel, C. Michel, S.-X. Liu, D. Schildbach, D. Fenske, *Eur. J. Inorg. Chem.* **2001**, *2001*, 1155–1166.
[52] S. De, K. Mahata, M. Schmittel, *Chem. Soc. Rev.* **2010**, *39*, 1555–1575.
[53] M. Schmittel, A. Ganz, *Chem. Commun.* **1997**, 999–1000.
[54] C. Chiorboli, M. A. J. Rodgers, F. Scandola, *J. Am. Chem. Soc.* **2003**, *125*, 483–491.
[55] C. Chiorboli, C. A. Bignozzi, F. Scandola, E. Ishow, A. Gourdon, J.-P. Launay, *Inorg. Chem.* **1999**, *38*, 2402–2410.
[56] C. T. Cunningham, K. L. H. Cunningham, J. F. Michalec, D. R. McMillin, *Inorg. Chem.* **1999**, *38*, 4388–4392.
[57] M. Ruthkosky, C. A. Kelly, F. N. Castellano, G. J. Meyer, *Coord. Chem. Rev.* **1998**, *171*, 309–322.
[58] M. W. Blaskie, D. R. Mcmillin, *Inorg. Chem.* **1980**, *19*, 3519–3522.
[59] L. X. Chen, G. Jennings, T. Liu, D. J. Gosztola, J. P. Hessler, D. V. Scaltrito, G. J. Meyer, *J. Am. Chem. Soc.* **2002**, *124*, 10861–10867.
[60] X. Qiu, J. W. Thompson, S. J. L. Billinge, *J. Appl. Crystallogr.* **2004**, *37*, 678.
[61] S. D. Bergman, M. Kol, *Inorg. Chem.* **2005**, *44*, 1647–1654.
[62] CCDC-2084517 (**Os-Cu**), 2084518 (**Os-Os**), and 2084519 (**Cu-Cu**) contain the supplementary crystallographic data for this paper. These data can be obtained free of charge from The Cambridge Crystallographic Data Centre via www.ccdc.cam.ac.uk/data_request/cif.
[63] S. D. Fairbanks, C. C. Robertson, F. R. Keene, J. A. Thomas, M. P. Williamson, *J. Am. Chem. Soc.* **2019**, *141*, 4644–4652.
[64] L. Yang, D. R. Powell, R. P. Houser, *J. Chem. Soc. Dalt. Trans.* **2007**, 955–964.
[65] L. Kohler, D. Hayes, J. Hong, T. J. Carter, M. L. Shelby, K. A. Fransted, L. X. Chen, K. L. Mulfort, *Dalt. Trans.* **2016**, *45*, 9871–9883.
[66] L. Kohler, R. G. Hadt, D. Hayes, L. X. Chen, K. L. Mulfort, *Dalt. Trans.* **2017**, *46*, 13088–13100.
[67] J.-D. Chai, M. Head-Gordon, *Phys. Chem. Chem. Phys.* **2008**, *10*, 6615–6620.
[68] P. J. Hay, W. R. Wadt, *J. Chem. Phys.* **1985**, *82*, 270–283.
[69] S. Miertuš, E. Scrocco, J. Tomasi, *Chem. Phys.* **1981**, *55*, 117–129.
[70] M. W. Mara, K. A. Fransted, L. X. Chen, *Coord. Chem. Rev.* **2015**, *282–283*, 2–18.
[71] S. E. Canton, K. S. Kjær, G. Vankó, T. B. van Driel, S. Adachi, A. Bordage, C. Bressler, P. Chabera, M. Christensen, A. O. Dohn, A. Galler, W. Gawelda, D. Gosztola, K. Haldrup, T. Harlang, Y. Liu, K. B. Møller, Z. Németh, S. Nozawa, M. Pápai, T. Sato, T. Sato, K. Suarez-Alcantara, T. Togashi, K. Tono, J. Uhlig, D. A. Vithanage, K. Wärnmark, M. Yabashi, J. Zhang, V. Sundström, M. M. Nielsen, *Nat. Commun.* **2015**, *6*, 1–10.
[72] E. Biasin, Z. W. Fox, A. Andersen, K. Ledbetter, K. S. Kjær, R. Alonso-Mori, J. M. Carlstad, M. Chollet, J. D. Gaynor, J. M. Glownia, K. Hong, T. Kroll, J. H. Lee, C. Liekhus-Schmaltz, M. Reinhard, D. Sokaras, Y. Zhang, G. Doumy, A. M. March, S. H. Southworth, S. Mukamel, K. J. Gaffney, R. W. Schoenlein, N. Govind, A. A. Cordones, M. Khalil, *Nat. Chem.* **2021**, *13*, 343–349.

Entry for the Table of Contents

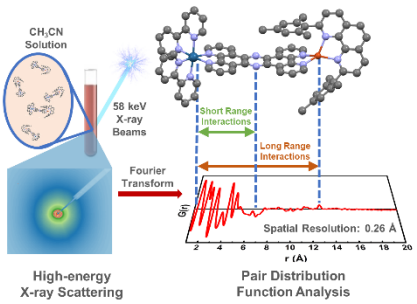

The solution phase structure of five bimetallic Ru(II)/Os(II)/Cu(I) complexes have been revealed by high-energy X-ray scattering and pair distribution function analysis (HEXS/PDF). Assisted by computational simulation, conformational differences of the complexes between solution and solid state were identified with sub-Angstrom resolution. This study demonstrates the potential application of HEXS/PDF to uncover the true solution phase structure and conformation of transition metal complexes.